RESEARCH ARTICLE

Macromolecular Rapid Communications
www.mrc-journal.de

Modulating the Crystallinity of a Circular Plastic towards Packaging Material with Outstanding Barrier Properties

Ainara Sangroniz, Jian-Bo Zhu, Agustin Etxeberria, Eugene Y.-X. Chen, and Haritz Sardon**

Chemically recyclable polymers have attracted increasing attention since they are promising materials in a circular economy, but such polymers appropriate for packaging applications are scarce. Here a combined thermal, mechanical, and transport (permeability and sorption) study is presented of a circular polymer system based on biobased *trans*-hexahydrophthalide which, upon polymerization, can lead to amorphous, homochiral crystalline, and nanocrystalline stereocomplex materials. This study uncovers their largely different transport properties of the same polymer but with different stereochemical arrangements and synergistic or conflicting effects of crystallinity on transport properties versus thermal and mechanical properties. Overall, the homocrystalline chiral polymer shows the best performance with an outstanding barrier character to gases and vapors, outperforming commercial poly(ethylene terephthalate) and polyethylene. The results presented herein show that it is possible to modify the crystalline structure of the same polymer to tune the mechanical and transport properties and generate multiple materials of different barrier characters.

1. Introduction

Polymers can be found in a wide range of applications such as civil engineering, biomedicine, automotive industry, and renewable energy. One of the most important applications of polymers is packaging, and in fact about 40% of them are used in this sector.[1] Packaging is of paramount importance to reduce the food waste, increase the lifetime of the products, and ensure the food quality and safety. However, the lifetime of single-use packaging material is short, and after a period of time it is disposed, thus contributing to the huge problem of plastic waste.[2]

A. Sangroniz, J.-B. Zhu, E. Y.-X. Chen
Department of Chemistry
Colorado State University
Fort Collins, CO 80523–1872, USA
E-mail: eugene.chen@colostate.edu

A. Sangroniz, A. Etxeberria, H. Sardon
POLYMAT
Department of Polymer Science and Technology
University of the Basque Country UPV/EHU
Manuel de Lardizabal, 3, Donostia 20018, Spain
E-mail: haritz.sardon@ehu.eus

The ORCID identification number(s) for the author(s) of this article can be found under https://doi.org/10.1002/marc.202200008

DOI: 10.1002/marc.202200008

In search for more sustainable materials, biodegradable polymers have garnered great attention in the last decades since they can be degraded to carbon dioxide, water and biomass.[3,4] However, some common biodegradable polymers such as polylactide (PLA) or polyhydroxybutyrate do not possess properties desired for packaging applications.[5,6] In some cases the degradation is too slow and the economic value of the postconsumer material is not recovered. Furthermore, the chemical recycling of these polymers does not lead to the starting monomer. A more promising approach to obtain sustainable polymers is the use of fully chemically recyclable, circular materials that can establish closed-loop lifecycles. In this case, after the disposal of packaging, the plastic waste can be converted to the original monomer or to new building blocks, thus no or minimum waste is generated, following the circular economy framework.[7,8] Although much effort has been made in search for novel chemically recyclable polymers,[9–17] the works covering the final properties, especially transport properties for packaging applications are scarce.[18]

The materials that are used in food packaging applications must meet different requirements depending on the packed product. For instance, for fruits and vegetables, a material that is permeable to carbon dioxide and oxygen has to be used without losing water. On the other hand, there are some products that need a high barrier character to carbon dioxide, for example, carbonated drinks where carbon dioxide should not scape the container.[19] Therefore, materials with a wide range of transport properties are needed depending on the specific application.

Usually, to achieve the required barrier properties different polymer layers are employed. For example, poly(ethyelene) that has a high water vapor barrier character is combined with polyamide or poly(vinyl alcohol) to improve its barrier character to oxygen. Although this approach allows to obtain materials with desired properties, it makes the recycling of the system more complex, difficult, time consuming, and expensive. Therefore, monocomponent systems with tunable mechanical and barrier properties are required that allow to achieve a wide range of properties by employing only one polymer. Indeed, this will simplify the recycling process as prior sorting of materials will not be required.

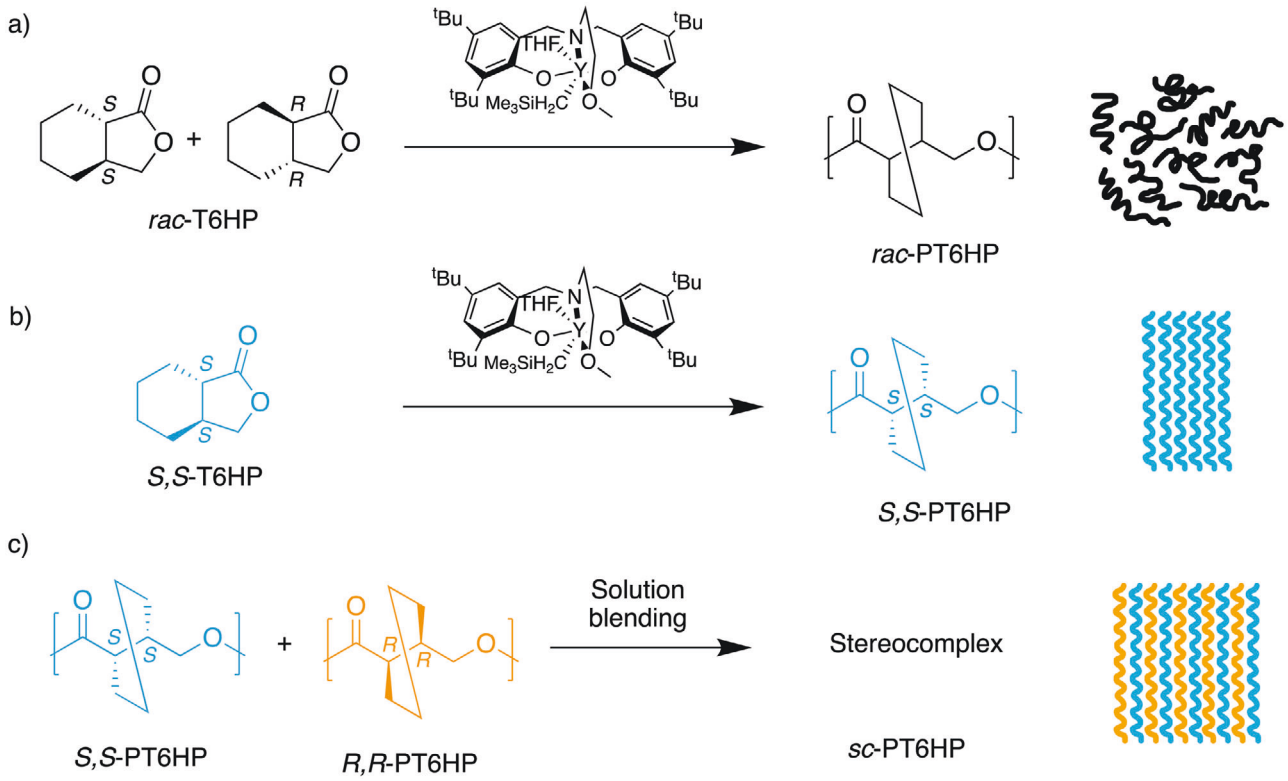

Scheme 1. Synthesis and preparation of a) *rac*-PT6HP (amorphous), b) *S,S*-PT6HP (homocrystal), and c) *sc*-PT6HP (stereocomplex) by blending *S,S*-PT6HP and *R,R*-PT6HP in a 1:1 ratio.

Transport properties of polymers are influenced by several factors such as the glass transition temperature (T_g), crystallinity, and free volume of the polymer, among others.[20] Bearing this in mind, one way to obtain monocomponent materials with different properties is to tune the crystallinity of the polymer by controlling its stereochemistry, as crystallinity impacts the polymer's T_g, melting-transition temperature (T_m), and free volume which, in turn, modulate its transport properties without changing the polymer's chemical composition or type. In fact, amorphous polymers show a higher permeability to gases and vapors than semicrystalline counterparts. In the case of semicrystalline materials, the penetrants cannot be solubilized in the crystals; therefore, the crystallites create a tortuous pathway for penetrants and thus decrease the diffusion coefficient and thus the permeability.[20] Stereocomplexation is a powerful strategy to enhance the thermal and mechanical properties of polymers.[21–23] Furthermore, it has recently been shown that stereocomplexation can be very efficient to improve the barrier character of PLA.[24,25] However, the works covering this issue are scarce and whether the results on the PLA stereocomplex could be extended to other polymers remains an unanswered question.

Among chemically recyclable polymers, those based on γ-butyrolactone are very promising since they can be obtained from renewable resources and are fully chemically recycled, in principle, infinitely. In particular, the *trans*-ring fused γ-butyrolactone, *trans*-hexahydrophthalide (T6HP), has been shown to be an intriguing monomer platform since coordination-insertion ring-opening polymerization of different T6HP stereoisomers or their mixtures with stereoselective catalysts has led to formation of either amorphous *rac*-PT6HP or homocrystalline chiral polymers *S,S*-PT6HP and *R,R*-PT6HP.[15,18] Furthermore, physical blending *S,S*-PT6HP with *R,R*-PT6HP in a 1:1 ratio led to a crystalline stereocomplex with a much higher T_m and faster crystallization rate than the parent enantiomeric polymers.[15] Therefore, this polymer system provides an excellent opportunity to examine the effect of the crystallinity (and its structure), or the lack thereof, on the mechanical and transport properties. Some of us reported previously that in the case of PLA, the homopolymer and stereocomplex show different transport properties.[24] In this contribution, we investigated the chemically circular PT6HP system and gained a deeper insight into the structure–property relationship among homocrystalline and stereocomplex polymers.

2. Results and Discussion

2.1. Synthesis of Amorphous and Crystalline PT6HP Materials

Amorphous *rac*-PT6HP, homochiral crystalline *S,S*-PT6HP, and stereocomplex *sc*-PT6HP were prepared since this set of PT6HP samples provides a unique opportunity to investigate effects of the crystallinity and stereocomplexation on mechanical and transport properties.

Scheme 1 outlines the synthesis of the above PT6HP samples. Amorphous and homochiral crystalline polymers were synthesized by the coordinative-insertion ring-opening polymerization of *rac*-T6HP, *R,R*-T6HP and *S,S*-T6HP monomers,

Table 1. Thermal properties of *rac*-PT6HP, *S,S*-PT6HP, and *sc*-PT6HP.

Samples	T_g [°C]	T_m [°C]	ΔH_{fus} [J g^{-1}]
rac-PT6HP	55	–	–
S,S-PT6HP	64	125.1	29
sc-PT6HP	60	192.0	26

respectively, using the yttrium based catalyst according to the literature procedures, see the spectrum in Figure S1 in the Supporting Information.[15] *rac*-PT6HP (M_n = 1110 kg mol^{-1}, $Đ$ = 1.09), *R,R*-PT6HP (M_n = 415 kg mol^{-1}, $Đ$ = 1.11), and *S,S*-PT6HP (M_n = 305 kg mol^{-1}, $Đ$ = 1.21) were obtained. The stereocomplex, *sc*-PT6HP, was obtained by blending *R,R*-PT6HP and *S,S*-PT6HP polymers in a 1:1 ratio, prepared by their respective enantiopure monomers.[15]

2.2. Thermal Properties of Amorphous and Crystalline PT6HP Materials

Thermal properties of *rac*-PT6HP, *S,S*-PT6HP, and *sc*-PT6HP have been examined by differential scanning calorimetry (DSC), since, as mentioned previously, they play an important role in their transport properties. The data have been collected from the first DSC heating scan and are shown in **Table 1**, see Figure S2 (Supporting Information) for the thermograms. It is worth noting here that, due to slow crystallization of homochiral *S,S*-PT6HP or *R,R*-PT6HP, no T_m can be observed on the second DSC heating scan, whereas *sc*-PT6HP retains its crystallinity.[15] However, in this study, PT6HP-based membranes for measuring transport barriers were prepared by solvent-casting, not by compression molding or hot-pressing; hence, their first DSC heating scan thermal transition data are directly related to their transport properties and thus recorded and analyzed.

The thermal analysis shows that both, *S,S*-PT6HP and *sc*-PT6HP samples are semicrystalline. Regarding the melting temperature of the crystallites, *S,S*-PT6HP shows a T_m of 125.1°C, whereas in the case of the stereocomplex the T_m increases up to 192.0 °C. This observation is consistent with the trend observed for other stereoregular polymers that are able to form the stereocomplex, for example PLA.[26]

The melting enthalpy is similar for both cases, 29 and 26 J g^{-1} for the homocrystal and stereocomplex, respectively. For other stereocomplex polymers reported in literature, the melting enthalpy of 100% crystalline polymer is higher for the stereocomplex than for the analogous homocrystalline polymer. For example, the melting enthalpy of 100% crystalline PLA is higher for the stereocomplex, ΔH°_{fus} = 142 J g^{-1}, than for the homocrystalline polymer, ΔH°_{fus} = 106 J g^{-1}.[27] The same trend was observed for poly(methyl methacrylate) stereocomplexes.[28] Thus, the observed lower ΔH°_{fus} for *sc*-PT6HP than *S,S*-PT6HP indicated a lower crystallinity for *sc*-PT6HP, despite having a much higher T_m, presumably a result of imperfect stereocomplexation between *S,S*-PT6HP and *R,R*-PT6HP chains likely due to sterics of the fused cyclohexyl ring on the main chain. This is in accordance with the T_g (vide supra); the homocrystal would have a higher crystallinity level which hinders the segmental mobility of the polymer chain leading to a higher T_g.

Table 2. Mechanical properties of *rac*-PT6HP, *S,S*-PT6HP, and *sc*-PT6HP.

Samples	Tensile strength [MPa]	Young modulus [MPa]	Elongation at break [%]
rac-PT6HP[a)]	26.2 ± 3.2	1850 ± 300	13.1 ± 3.5
S,S-PT6HP	35.2 ± 0.6	3890 ± 320	1.5 ± 0.4
sc-PT6HP[a)]	54.7 ± 4.0	2720 ± 250	6.5 ± 1.2

[a)] reported in ref. [15].

Thermal analysis showed that the T_g of the amorphous *rac*-PT6HP is 55 °C. The T_g of the homocrystalline *S,S*-PT6HP increases to 64 °C, whereas the T_g of the stereocomplex *sc*-PT6HP exhibits an intermediate value of 60 °C. It is worth noting that the T_g spans over 9 °C depending on the crystallinity, which should notably impact their transport properties. The higher T_g of the semicrystalline materials arises from the constraining effect of the crystallites that hinder the mobility of the amorphous chains.

2.3. Mechanical Properties of Amorphous and Crystalline PT6HP Materials

Mechanical properties of the above three samples were measured, and the results were summarized in **Table 2**. As anticipated, the amorphous *rac*-PT6HP shows the lowest tensile strength and Young modulus, whereas it has the highest elongation at break. The homocrystalline *S,S*-PT6HP exhibits the highest Young modulus, an intermediate tensile strength, and the lowest elongation at break. Interestingly, within this series the stereocomplex possesses the highest tensile strength, but an intermediate Young modulus and an intermediate elongation at break.

From these results it can be concluded that the amorphous *rac*-PT6HP shows the lowest tensile performance but the highest ductility, as expected. Semicrystalline samples present a higher tensile stress and Young modulus due to the presence of rigid crystals that lead also to a reduction in the elongation at break. The stereocomplex shows slightly better overall properties than the homocrystalline sample. In the case of PLA, it has also been reported that the Young modulus is slightly lower for the stereocomplex in comparison to the homocrystalline poly(L-lactide) (PLLA), depending on processing conditions.[27,29–31] In addition, both the tensile strength and elongation at break were reported to be higher for the stereocomplex in the case of PLA. Therefore, the results obtained for this system are in agreement with the findings for PLA.

2.4. Transport Properties of Amorphous and Crystalline PT6HP Materials

To examine the effect of the crystallinity and crystalline structure on the transport properties, the permeability to water vapor, oxygen, and carbon dioxide was measured for the three amorphous and crystalline PT6HP samples. The water vapor transmission rate (WVTR) is shown in **Figure 1**, and the values are reported in Table S1 in the Supporting Information. As it can be seen *S,S*-PT6HP shows an excellent barrier character towards water

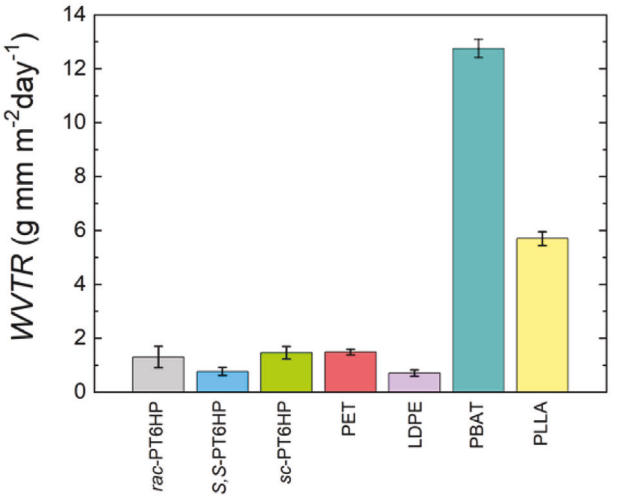

Figure 1. Water vapor transmission rates of *rac*-PT6HP, *S,S*-PT6HP, and *sc*-PT6HP, as compared to commercial packaging materials PET, LDPE, PBAT, and PLLA.

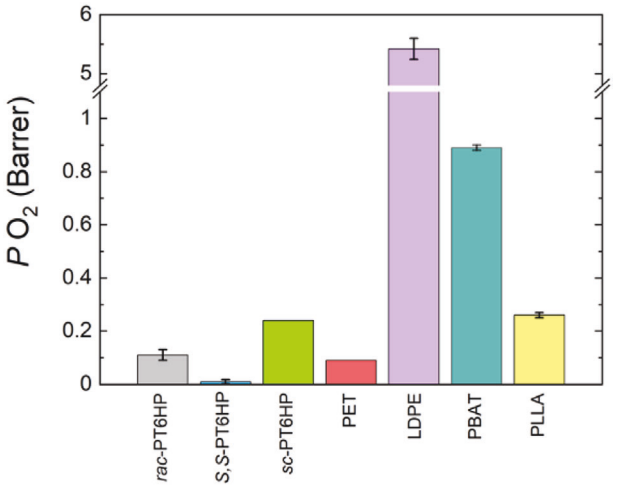

Figure 2. Oxygen permeability of *rac*-PT6HP, *S,S*-PT6HP, and *sc*-PT6HP, as compared to commercial packaging materials PET, LDPE, PBAT, and PLLA.

vapor, with an extremely low value of 0.77 ± 0.15 g mm m^{-2} day^{-1}, which is similar to that of low density polyethylene (LDPE) (0.71 g mm m^{-2} day^{-1}) and lower than that of poly(ethylene terephthalate) (PET) (1.49 g mm m^{-2} day^{-1}).[32] *sc*-PT6HP and *rac*-PT6HP show higher values of 1.46 and 1.30 g mm m^{-2} day^{-1}, respectively, which are still comparable with that of PET and much lower than those of poly(butylene adipate-co-terephthalate) (PBAT)[33] (12.8 g mm m^{-2} day^{-1}) and PLLA[24] (5.7 g mm m^{-2} day^{-1}). These results indicate that the sample with the highest T_g (*S,S*-PT6HP, 64 °C) and the highest crystallinity within this PT6HP series exhibits the lowest water vapor permeability attributable to its lowest chain mobility.

rac-PT6HP shows a slightly higher permeability (1.30 ± 0.40 g mm m^{-2} day^{-1}) with a T_g of 55 °C, and a slightly higher permeability was observed for *sc*-PT6HP (1.46 ± 0.23 g mm m^{-2} day^{-1}) that has a higher T_g of 60 °C. In any case, the values of the amorphous and stereocomplex samples are comparable taking into account the standard deviation. This result is unexpected since *sc*-PT6HP is semicrystalline and, as mentioned previously, the crystallites reduce the permeability and, thus, it should give a lower permeability than the amorphous polymer. One possible explanation for that could be due to the crystalline structure of the stereocomplex, the lower crystallinity, and the smaller size of the crystallites (nanocrystallites) compared to the much larger homocrystals.[34] The smaller size of the crystallites in the case of the stereocomplex leads to a higher interphase which could create a higher free volume and thus facilitate the diffusion of the penetrant (vide infra). However, if the density of the samples is analyze, see Table S2 (Supporting Information), it increases following this trend: *rac*-PT6HP < *S,S*-PT6HP < *sc*-PT6HP. Therefore, there must be another reason that leads to these results. The Wide Angle X-ray Scattering (WAXS) data, see Figure S3 (Supporting Information), shows that the crystalline structures of *S,S*-PT6HP and *sc*-PT6HP are different. The stereocomplex shows a new peak at 8.0° and the peaks at about 11.4° disappear. A similar trend is observed also in homocrystalline and stereocomplex PLLA.[30] It could be possible that the crystalline structure of the stereocomplex is more open leading to a higher permeability values. Also unexpected results have been obtained in unique polymers, were the increase of the crystallinity level led to an increase in the permeability due to the open crystal structure.[35] Overall, the permeability results are opposite to those obtained in the case of PLA, in which the stereocomplex exhibited better barrier properties than the homocrystal.[24,25] The discussion will ensue after analyzing the carbon dioxide sorption results.

Figure 2 shows the oxygen permeability results, with values collected in Table S1 in the Supporting information. The lowest value is obtained again for the homocrystalline sample *S,S*-PT6HP, 0.01 Barrer, showing an outstanding barrier character that is 9 times lower than that of PET. In the case of the amorphous *rac*-PT6HP, the permeability is one order of magnitude higher than the homocrystalline polymer and even a higher value is obtained for the stereocomplex. The trend observed is similar to that obtained for the WVTR. Therefore, as discussed previously, there are several factors that could account for this result, including the crystalline structure, the percent crystallinity, and the interphase between the crystallites and the amorphous phase.

To shed light on the obtained WVTR and oxygen permeability results, carbon dioxide sorption experiments were performed and solubility and diffusion coefficients were obtained. Carbon dioxide sorption isotherms are shown in **Figure 3** and Table S3 (Supporting Information). The amorphous *rac*-PT6HP shows the highest carbon dioxide sorption, followed by *S,S*-PT6HP and *sc*-PT6HP. At low pressures, in all the samples the concentration of carbon dioxide is proportional to pressure until 7.5 bar, therefore they follow Henry's law in this low pressure regime. At higher pressures the isotherms turn up slightly due to the plasticization effect, deviating positively from the Henry type law. The plasticization effect of carbon dioxide at high pressures has been reported widely in literature.[36–38] From the obtained results, it seems that the plasticization effect is more significant for *S,S*-PT6HP sample.

The solubility coefficient is shown in Figure S4 (Supporting Information). *sc*-PT6HP shows the lowest value, whereas

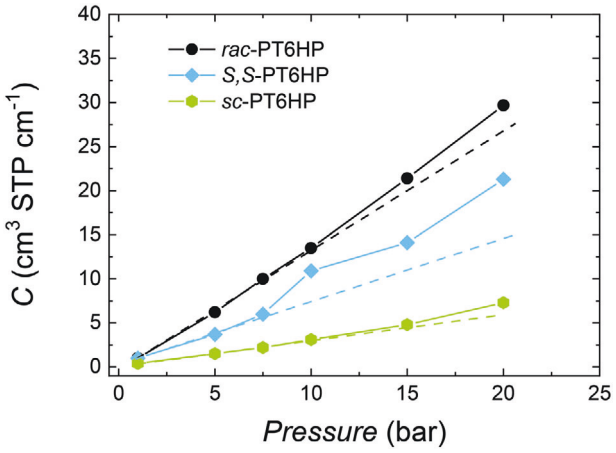

Figure 3. Carbon dioxide sorption isotherms of *rac*-PT6HP, *S,S*-PT6HP, and *sc*-PT6HP.

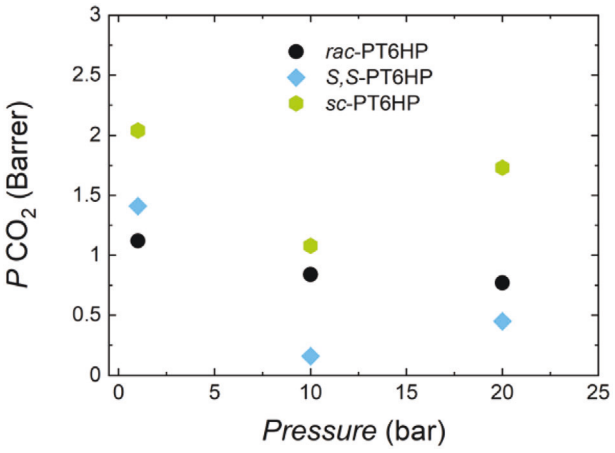

Figure 5. Permeability coefficients of *rac*-PT6HP, *S,S*-PT6HP, and *sc*-PT6HP.

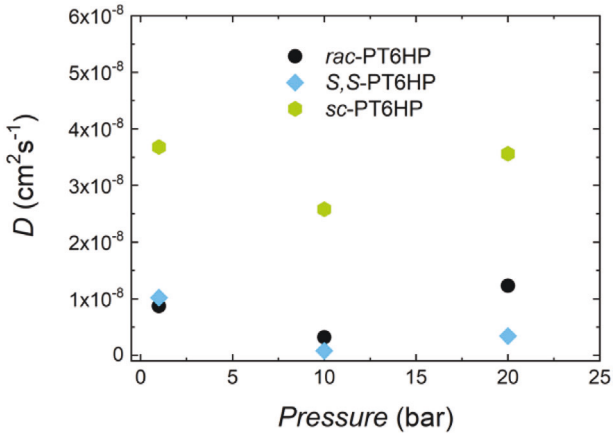

Figure 4. Diffusion coefficients of *rac*-PT6HP, *S,S*-PT6HP, and *sc*-PT6HP.

rac-PT6HP and *S,S*-PT6HP present a solubility coefficient that is practically one order of magnitude higher. The formation of a stereocomplex arises from the formation of intermolecular hydrogen bonds between two enantiopure polymer chains.[25–27,39] It is possible that the interactions between the chains are stronger in the stereocomplex, therefore weaker interactions could be formed with the penetrant, which would lead to lower solubility coefficient values.

Diffusion coefficients are summarized in **Figure 4** and Table S4 (Supporting Information). The lowest values are obtained for *rac*-PT6HP and *S,S*-PT6HP, whereas *sc*-PT6HP shows the highest values. From these results it can be stated that the free volume fraction in the stereocomplex is much higher than in the homocrystalline and the amorphous samples. The presence of crystallites in the stereocomplex does not lead to a lower diffusion coefficient. This could arise, as mentioned previously, from the low crystallinity level, the crystalline structure and the small size of the crystallites that lead to a higher amount of interphase which has probably a higher free volume and thus facilitates the diffusion of the penetrant. The higher free volume possessed by the stereocomplex PT6HP could also explain why in this case the transport results obtained are the opposite than the ones obtained for homocrystalline and stereocomplex PLA materials.[24,25]

By analyzing the diffusion coefficient over pressure, it can be seen that in all the cases the diffusion coefficient decreases with pressure, reaching the lowest value at 10 bar. The decrease of the diffusion coefficient at 10 bar results from the competition between molecules, whereas when the pressure is increased to 20 bar, an increase of diffusion occurs due to the plasticization.

The CO_2 permeability coefficients for the three PT6HP samples over the pressure are shown in **Figure 5**, with the data reported in Table S5 (Supporting Information). *sc*-PT6HP shows the highest permeability with a value of 2.0 Barrer. *rac*-PT6HP and *S,S*-PT6HP exhibit similar permeability values of 1.1 and 1.4, Barrer, respectively. This behavior is practically the same as that obtained for WVTR and oxygen permeability described above.

In the case of *rac*-PT6HP the permeability decreases as the pressure rises whereas *S,S*-PT6HP and *sc*-PT6HP show a different behavior: the permeability decreases at 10 bar and it rises slightly at 20 bar, due to the plasticization effect. Probably, due to their semicrystalline nature and the higher glass transition temperature, the pressure range studied is enough to achieve the plasticization of the sample, whereas in the case of *rac*-PT6HP higher pressures could be needed.[40]

3. Conclusion

In this contribution we report a chemically recyclable, circular plastic system with tunable thermal, mechanical, and transport properties by changing the stereochemistry that brings about different crystalline structures. The presence of crystallites renders melting transitions and increases the glass transition temperature and the tensile-related mechanical properties (Young modulus and tensile strength). Regarding transport properties, the homocrystalline *S,S*-PT6HP material presents the highest barrier character, being better than PET and LDPE for both water vapor and oxygen permeability. On the other hand, the stereocomplexed *sc*-PT6HP, despite being crystalline, shows the highest permeability values, attributed to a higher free volume. This unexpected result could arise from the low melting enthalpy, the

crystalline structure, and the smaller size of the crystallites that increase the interphase between the crystalline and amorphous regions. The results obtained from the system studied here indicate that the stereocomplexation, which often presents a powerful strategy to enhance materials thermal and mechanical properties, is not always a good strategy to achieve a high barrier material, opposite to the findings of PLA.

4. Experimental Section

Synthesis of Homopolymers and Copolymers: The monomers and polymers were synthetized following the procedure described previously.[15,18] The polymerization reactions were performed in 25 mL Schlenk flask at 25 °C under inert atmosphere in the glove box. To the stirring monomer the catalyst was incorporated and after the appropriate period of time the reaction was quenched by the addition of acidified chloroform with HCl (5%). The solution was precipitated in excess cold methanol, filtered and washed again with cold methanol. The procedure was repeated 2 times to ensure the removal of unreacted monomer and catalyst. The obtained polymer was dried at 60 °C under vacuum, for three days.

Preparation of Membrane Samples: The membranes were prepared by solvent casting employing chloroform as the solvent. The polymer (0.2 g) was dissolved in chloroform (7 mL) and stirrer for 14 h. In the case of the stereocomplex isotactic *R,R*-PT6HP and *S,S*-PT6HP polymers were mixed in 1:1 molar ratio. Then chloroform was added and it was stirred for 14 h. The polymer solution was poured onto a petri dish. After 24 h at room temperature, it was dried in an oven at 70 °C for 2 d under vacuum and 4 more days at room temperature under vacuum. The thickness of the films was in the range of 50–100 µm.

Thermal Analysis: The thermal properties were analyzed by differential scanning calorimetry (DSC) employing a calorimeter from TA Instruments, model Q2000 V24. The samples of approximately 3 mg were encapsulated in aluminum pans. The materials were heated from −80 to 200 °C (to 225 °C in the case of the stereocomplex) at a heating rate of 10 °C min^{-1}.

Density Characterization: The density measurements were performed in a gradient density column, employing NaBr aqueous solution at 23 °C. The density values reported are the average of three samples.

WAXS: X-ray diffraction patterns were recorded in a PHILIPS X'PERT PRO automatic diffractometer in theta-theta configuration, secondary monochromator with Cu Kα radiation (λ = 1.5418 Å) and employing a PIXcel solid state detector. The conditions were: scan of $2\theta = 5$–60 with a step size of 0.05 and count time of 20 sec per step at 25 °C.

Characterization of Mechanical Properties: The mechanical properties corresponding to *S,S*-PT6HP sample were characterized by a Instron 5565 testing machine (Norwood, MA, USA) at a crosshead displacement rate of 5 mm min^{-1} at 22 °C. The specimens were cut according to ASTM D638 type V and have a thickness of 100–150 µm. 4 specimens were tested for the reported value.

Characterization of Transport Properties: Water vapor transmission rate was characterized employing the gravimetric method at 25 °C. The poly(tetrafluoroethylene) permeation cell was partially filled with water, and a membrane was placed above it sealing its top. The water vapor permeates through the membrane and evaporates into the air. The cell was placed in a Sartorius analytical balance with a readability of 10^{-5} g.[33,41–43] The weight loss was recorded in a computer for further data treatment. The values shown here are the average of at least 5 measurements.

Oxygen permeability was measured employing a Mocon Ox-Tran 2/21 MH model equipment. The measurements were performed at 23 °C, 1 atm and under dry conditions.[42,43]

Carbon dioxide sorption kinetics were measured with a Hiden IGA-2 electrobalance. The measurements were performed at 1, 5, 7.5, 10, 15, and 20 bar and 25 °C. Analyzing properly the data solubility and diffusion coefficients (*S* and *D*, respectively) can be determined. The absorbed gas concentration (*C*) was calculated from the equilibrium weight gain (M_∞) of the membrane by means of Equation 1

$$C\left[\frac{cm^3 STP}{cm^3}\right] = \frac{22414 \times M_\infty}{44 \times V_{plm}}$$

where V_{plm} is the volume occupied by the sample, in cm^3; M_∞, the total absorbed mass at equilibrium in g; and 44 g mol^{-1}, the molecular weight of carbon dioxide. The solubility coefficient, *S*, is given by Equation 2

$$S = \frac{C}{p}$$

where *p* is the pressure. To obtain the diffusion coefficient, Fick's second law must be solved, which depends on the geometry and concentration. The mass uptake of the penetrant is described by Equation 3, taking into account that in a thin membrane the edge of the membrane can be considered negligible and assuming that the pressure of the penetrant and the diffusion coefficient are constant

$$\frac{M_t}{M_\infty} = 1 - \frac{8}{\pi}\sum_{n=0}^{\infty}\frac{1}{(2n+1)^2}\exp\left(-\frac{D(2n+1)^2\pi^2 t}{l^2}\right)$$

where M_t is the absorbed gas at *t* time; *l*, the film thickness; and *D*, the diffusion coefficient (in cm^2 s^{-1}). This equation can be simplified leading to the so-called short time (up to 50% of $M\infty$) and longtime approximation (50–90% of M_∞).[44]

Supporting Information

Supporting Information is available from the Wiley Online Library or from the author.

Acknowledgements

This work was supported by the Basque Country Government (GC IT-1313-19), the Spanish Ministry of Innovation and Competitiveness EUR2020/112080 and BBVA Foundation for the Leonardo Grant 2020, and the U.S. National Science Foundation (NSF-1664915 and NSF-1955482) for the work performed at Colorado State University. A.S. thanks the Basque Government for the postdoctoral fellowship (POSDOC).

Conflict of Interest

E.Y.-X.C. and J.-B.Z. are inventors on U.S. Pat. 10,759,899 B2, 2020 submitted by Colorado State University Research Foundation, which covers the herein described recyclable polymer system and its stereocomplexes. The other authors declare no conflict of interest.

Data Availability Statement

The data that support the findings of this study are available in the supplementary material of this article.

Keywords

chemically recyclable polymers, circular plastics, packaging, transport properties

Received: January 4, 2022
Revised: February 8, 2022
Published online:

[1] Plastics PlasticsEurope, *The Facts: an Analysis of European Plastics Production, Demand and Waste Data*, PlasticsEurope, **2021**, https://plasticseurope.org/wp-content/uploads/2021/12/Plastics-the-Facts-2021-web-final.pdf. (Accessed: Feb 2021).
[2] World Economic Forum, Ellen MacArthur Foundation, and McKinsey & Company, The New Plastics Economy: Rethinking the Future of Plastics (Ellen MacArthur Foundation, 2016), https://www.ellenmacarthurfoundation.org/publications/the-new-plastics-economy-rethinking-the-future-of-plastics. (Accessed: Feb 2021).
[3] R. A. Gross, B. Kalra, *Green Chem.* **2002**, *297*, 803.
[4] V. Siracusa, P. Rocculi, S. Romani, M. D. Rosa, *Trends Food Sci. Technol.* **2008**, *19*, 634.
[5] U. Sonchaeng, F. Iñiguez-Franco, R. Auras, S. Selke, M. Rubino, L. T. Lim, *Prog. Polym. Sci.* **2018**, *86*, 85.
[6] A. Chaos, A. Sangroniz, A. Gonzalez, M. Iriarte, J. R. Sarasua, J. del Río, A. Etxeberria, *Polym. Int.* **2019**, *68*, 125.
[7] C. Jehanno, M. M. Pérez-Madrigal, J. Demarteau, H. Sardon, A. P. Dove, *Polym. Chem.* **2019**, *10*, 172.
[8] X. Tang, E. Y.-X. Chen, *Chem* **2019**, *5*, 284.
[9] K. Stridsberg, A. C. Albertsson, *J. Polym. Sci., Part A: Polym. Chem.* **1999**, *37*, 3407.
[10] Y. Liu, H. Zhou, J. Z. Guo, W. M. Ren, X. B. Lu, *Angew. Chem., Int. Ed.* **2017**, *56*, 4862.
[11] M. Hong, E. Y.-X. Chen, *Nat. Chem.* **2016**, *8*, 42.
[12] M. Hong, E. Y.-X. Chen, *Angew. Chem., Int. Ed.* **2016**, *55*, 4188.
[13] J. P. MacDonald, M. P. Shaver, *Polym. Chem.* **2016**, *7*, 553.
[14] D. K. Schneiderman, M. E. Vanderlaan, A. M. Mannion, T. R. Panthani, D. C. Batiste, J. Z. Wang, F. S. Bates, C. W. Macosko, M. A. Hillmyer, *ACS Macro Lett.* **2016**, *5*, 515.
[15] J.-B. Zhu, E. M. Watson, J. Tang, E. Y.-X. Chen, *Science* **2018**, *360*, 398.
[16] H. Sardon, A. P. Dove, *Science* **2018**, *360*, 380.
[17] J.-B. Zhu, E. Y.-X. Chen, *Angew. Chem., Int. Ed.* **2018**, *57*, 12558.
[18] A. Sangroniz, J.-B. Zhu, X. Tang, A. Etxeberria, E. Y.-X. Chen, H. Sardon, *Nat. Commun.* **2019**, *10*, 3559.
[19] W. J. Koros, *Barrier Polymers and Structures*, American Chemical Society, Washington, D.C., USA **1990**.
[20] Y. Yampolskii, I. Pinnau, B. D. Freeman, *Materials Science of Membranes for Gas and Vapor Separation*, John Wiley and sons, Ltd, London, UK **2006**.
[21] Z.-Q. Wan, J. M. Longo, L.-X. Liang, H.-Y. Chen, G.-J. Hou, S. Yang, W.-P. Zhang, G. W. Coates, X.-B. Lu, *J. Am. Chem. Soc.* **2019**, *141*, 14780.
[22] D. Bandelli, J. Alex, C. Weber, U. S. Schubert, *Macromol. Rapid. Commun.* **2020**, *41*, 1900560.
[23] J. C. Worch, H. Prydderch, S. Jimaja, P. Bexis, M. L. Becker, A. P. Dove, *Nat. Rev. Chem.* **2019**, *3*, 514.
[24] A. Sangroniz, A. Chaos, M. Iriarte, J. del Río, J. R. Sarasua, A. Etxeberria, *Macromolecules* **2018**, *51*, 3923.
[25] H. Tsuji, T. Tsuruno, *Macromol. Mater. Eng.* **2010**, *295*, 709.
[26] J. R. Srasua, N. López Rodríguez, A. López Arraiza, E. Meaurio, *Macromolecules* **2005**, *38*, 8362.
[27] H. Tsuji, Y. Ikada, *Polymer* **1999**, *40*, 6699.
[28] K. Könnecke, G. Rehage, *Makromol. Chem.* **1983**, *184*, 2679.
[29] N. López-Rodríguez, I. M. Martínez de Arenaza, E. Meaurio, J. R. Sarasua, *J. Mech. Behav. Biomed. Mater.* **2014**, *37*, 219.
[30] H. Tsuji, *Macromol. Biosci.* **2005**, *5*, 569.
[31] J. R. Srasua, A. López-Arraiza, P. Balerdi, I. Maiza, *Polym. Eng. Sci.* **2005**, *45*, 745.
[32] L. Sangroniz, J. L. Ruiz, A. Sangroniz, M. Fernandez, A. Etxeberria, A. J. Müller, A. Santamaria, *J. Appl. Polym. Sci.* **2019**, *136*, 46986.
[33] A. Sangroniz, L. Sangroniz, N. Aranburu, M. Fernández, A. Santamaria, M. Iriarte, A. Etxeberria, *Eur. Polym. J.* **2018**, *105*, 348.
[34] Y. Furuhashi, Y. Kimura, N. Yoshie, *Polym. J.* **2006**, *38*, 1061.
[35] A. C. Puleo, D. R. Paul, P. K. Wong, *Polymer* **1989**, *30*, 1357.
[36] S. Kanehashi, T. Nakagawa, K. Nagai, X. Duthie, S. Kentish, G. Stevens, *J. Membrane Sci.* **2007**, *298*, 147.
[37] R. S. K. Valappil, N. Ghasem, M. Al-Marzouqi, *J. Ind. Eng. Chem.* **2021**, *98*, 103.
[38] M. Minelli, S. Oradei, M. Fiorini, G. C. Sarti, *Polymer* **2019**, *163*, 29.
[39] Z. Gu, Y. Xu, Q. Lu, C. Han, R. Liu, Z. Zhou, T. Hao, Y. Nie, *Phys. Chem. Chem. Phys.* **2019**, *21*, 6443.
[40] A. Bos, I. G. M. Pünt, M. Wessling, H. Strathmann, *J. Membr. Sci.* **1999**, *155*, 67.
[41] O. Miguel, J. J. Iruin, M. J. Fernandez-Berridi, *J. Appl. Polym. Sci.* **1997**, *64*, 1849.
[42] E. Lizundia, J. L. Vilas, A. Sangroniz, A. Etxeberria, *Eur. Polym. J.* **2017**, *91*, 10.
[43] A. Sangroniz, L. Sangroniz, A. Gonzalez, A. Santamaria, J. Del Río, M. Iriarte, A. Etxeberria, *Eur. Polym. J.* **2019**, *115*, 76.
[44] J. S. Crank, *The Mathematics of Diffusion*, 2nd ed., Clarendon Press, Oxford, UK **1975**.